Chaotic dynamics of inertial particles in three-dimensional rotating flows

Cristian Escauriaza*
School of Civil and Environmental Engineering
Georgia Institute of Technology,
Atlanta, GA 30332-0355, U.S.A
(Dated: May 2, 2005)

Transport and mixing problems in non-turbulent flows have been studied with chaotic advection theory to understand and quantify the characteristics of the fluid particle dynamics in simple analytical flows, and new analyses have been recently extended to realistic and more complex, experimentally realizable flows. Many environmental and engineering flows have also two or more phases, but little progress has been made in understanding the properties of these flows when there are inertial particles within the fluid. The purpose of this research is to study numerically the dynamics of inertial particles in a three-dimensional flow inside a closed cylinder with exactly counter-rotating lids. The one-way coupling simulations are based on analytical models of the forces acting on the particles, and on a simple elastic collision scheme with the boundaries. The solutions show how the effect of gravity can suppress the chaotic motion observed in fluid particles due to sedimentation. Particle dynamics without gravity force is also analyzed through Lagrangian average maps and particle variance of concentration, confirming the effect of inertia that decreases mixing in the container. Additionally, from periodic orbit theory we evaluate a global average of the flow such as particle dispersion, based on the spectrum of the orbits obtained from the determinant calculated with few prime cycles of the system.

PACS numbers: 95.10.Fh, 47.11.+j, 47.52.+j, 45.70.Mg, 05.45.-a
Keywords: chaotic advection, Lagrangian particle tracking, two-phase flows, computational fluid dynamics

Georgia Tech PHYS 7224:
CHAOS, AND WHAT TO DO ABOUT IT
course project, spring semester 2005
advisor: F. Sotiropoulos

I. INTRODUCTION

Mixing in non-turbulent flows has been the subject of extensive study in recent years, since several geophysical and engineering flows exhibit chaotic dynamics due to stirring produced by continuous stretching and folding of material lines [1]. Chaotic advection theory [2] has been developed to analyze these transport and mixing problems, connecting nonlinear dynamics with fluid mechanics, based on the phase-space defined by the Lagrangian representation of fluid particles that show local instability and global mixing of trajectories.

The theoretical framework to describe these flows was first developed to study idealized two and three-dimensional flows, which were specified analitically as solutions of simplified Navier-Stokes equations [3–5]. Several experiments have also been carried out to elucidate the chaotic advection mechanisms driven by vortical structures in the flowfield, which homogenize the concentration of passive scalars [6–8].

Recently, investigations of experimentally realizable three-dimensional flows have given new insights in chaotic mixing of non-diffusive particles. The mechanisms of the rich Lagrangian dynamics of three-dimensional vortex breakdown bubbles in closed cylindrical containers have been studied in numerical and experimental investigations [9, 10], establishing the non-dimensional parameters that determine the Lagrangian characteristics of the flow.

The instability of the flow in a cylindrical container with exactly counter-rotating lids, also called *von Karman swirling flow*, was recently computed and studied in detail [11], identifying the chaotic characteristics of the flow at different Reynolds numbers. Numerical simulations agreed with stability analyses performed previously for this flow [12, 13]. The results [11] also showed how the shear-layer at the center of the container becomes unstable to azimuthal modes and developes radial and axial vortices, determining the onset of three-dimensional chaotic dynamics, while few stable/elliptic periodic orbits remain in islands or within toroidal regions close to the lids. From the flow instability, stationary radial *cat-eye* vortices emerge at the center of the container, in a number equivalent to the most unstable azimuthal wavenumber of the flow depending on the aspect ratio of the container, and the Reynolds number of the flow.

A remarkable finding of this study was the relationship established between the Reynolds number and the intensity of chaotic stirring. As the Reynolds number increases, the mixing increases up to a threshold, after which regions ocuppied by the unmixed islands grow, decreasing the stirring intensity within the flow. This phenomenon was previously studied [14], establishing that for steady and stable, bounded three-dimensional flows, mixing increases as long as viscous terms are important. If the Reynolds number is too large, and the flow re-

*Electronic address: gtg834i@prism.gatech.edu

mains steady, the chaotic regions and mixing in the flow will decrease.

Despite all this progress in Lagrangian studies of realistic complex three dimensional flows, there have been few investigations relating chaotic mixing of discrete inertial particles.

Particle-laden flows cover a wide range of applications in combustion, sprays, bubbly flows, atmospheric flows, and sediment transport in aquatic enviroments.

Numerical investigations of the Lagrangian properties of inertial particles in these flows have to take into account that solid particles cannot be considered passive scalars, but as a dispersed phase, which is subject to surface and body forces, as well as collisions with solid boundaries or other particles.

Most of the previous studies have been performed in analytical two-dimensional cellular flows or shear-layers. Numerical simulations have found that chaotic behavior of inertial particles depends on the density ratio between the two phases, and on the relative response time of the particles with respect to the time-scale of the vortical structures of the flow [15].

Recently, inertial particles in two-dimensional unsteady flows were analyzed in Hamiltonian systems [16], using the stream function of Kelvin's cat-eyes vortices, for which chaotic dynamics was only observed in heavy particle systems.

The aim of this research is to investigate numerically the three-dimensional steady flow in a cylindrical container with two exactly counter-rotating lids as shown in Fig. 1, comparing the results obtained in the calculations for passive non-diffusive fluid particles [11].

The simulated particle trajectories will allow us to determine the non-dimensional parameters that characterize the chaotic behavior of the particle system, and the particle dispersion for this particular flow from periodic orbit theory [17].

In sect. II the equations which govern the particle motion are derived by separating the effects of the different forces acting on the system. Implementation of the model with a critical analysis of the results unveiling the effect of inertia is presented in sect. III Results are summarized and discussed in sect. IV.

II. PROBLEM FORMULATION

The steady incompressible flow in a cylindrical container of radius R and height H, with lids rotating at the same angular velocity magnitude, Ω, but in opposite directions, as shown in Fig. 1, is characterized by two non-dimensional parameters: the Reynolds number, defined as:

$$Re = \frac{\Omega R^2}{\nu} \tag{1}$$

and the aspect ratio of the container:

$$AR = H/R \tag{2}$$

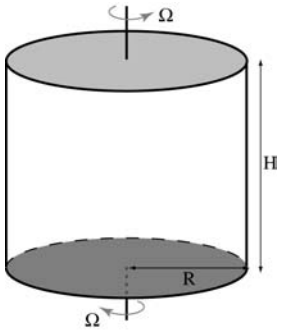

FIG. 1: Flow in a cylidrical container with counter-rotating lids.

The basic axisymmetric flow is formed by an invariant region of two tori where only quasi-periodic orbits of fluid particles exist. The upper and lower halves of the cylinder have recirculating patterns due to Ekman pumping, and the radial jet formed at the center of the container creates a shear layer, which is the mechanism responsible for the initiation of chaotic mixing.

Recent studies of this flow for different Reynolds numbers, aspect ratios, and angular velocities of the lids [12, 13, 18, 19], have shown that this azimuthal shear layer becomes unstable, exciting three-dimensional modes that break the symmetry of the flow.

Lackey [11] carried out numerical simulations for $AR = 1$, in a range of Reynolds numbers between 295 and 850, integrating the three-dimensional incompressible Navier-Stokes equations with a second-order accurate scheme, using $81 \times 211 \times 161$ grid nodes in cylindrical coordinates. Fig. 2 shows the solution at $Re = 350$, for which the azimuthal mode 3 is excited. The two isosurfaces of radial velocity evidence the three-dimensionality of the flow produced by the radial vortices, whose centers are stable foci on the azimuthal plane. For larger Reynolds numbers, these characteristics of the flow are more evident as it is further discussed in [11].

Fluid particle trajectories from a Lagrangian viewpoint can identify the invariant and chaotic regions within the flow to observe the global stirring effect as a function of the Reynolds number. Through Lagrangian average maps, the simulations showed that new invariant regions appear for $Re > 500$, reducing the size of the mixing area. The stirring intensity was quantified by the variance of concentration, which demonstrated that as long as the flow remains steady, there is a Reynolds number that maximizes stirring. Above this value the mixing declines approximately at $Re^{-1/2}$, confirming the theory developed by Mezić [14].

To explore the two-phase dynamics and interactions with the chaotic regions produced by the shear layer, we study numerically the motion of dispersed solid particles in this flow, by integrating their momentum equations.

Chaotic motion of inertial non-diffusive particles has only been studied for two-dimensional cell flows and ABC

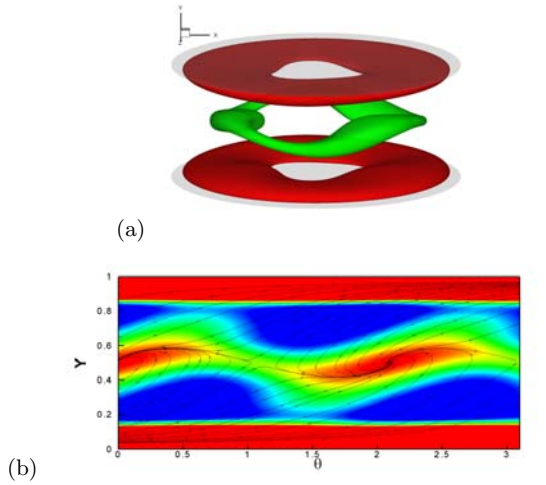

FIG. 2: Fully three-dimensional flowfield at $Re = 350$ and $AR = 1$ [11]. (a) Isosurfaces of radial velocity $u_r = -0.1\Omega R$ and $u_r = 0.065\Omega R$, and (b) Contours of radial vorticity, ω_r, and surface streamlines on the unfolded azimuthal plane $Y-\theta$ at $r = 0.75R$, $0 \leq \theta \leq \pi$.

flows [15, 16, 23–25]. The chaotic behavior of inertial particles is related to the ratio between the particle response time, which is a function of the drag force, and the characteristic time of the flow, as well as the density ratio between both phases.

These findings, however, have not been demonstrated in realistic three-dimensional flows. In this research we model the particle dynamics for the first time in experimentally realizable three-dimensional flows, using the solutions obtained for the cylinder with exactly counter-rotating lids.

To simulate the stirring of inertial dispersed particles that move independently of fluid elements, we need to establish the dynamic equations by modeling the forces acting on each particle. Therefore, the trajectory and momentum are described by the following system of equations:

$$\frac{dx_{pi}}{dt} = v_{pi} \tag{3}$$

$$m\frac{dv_{pi}}{dt} = f_i \tag{4}$$

where v_{pi} and x_{pi} are the velocity and the position of the particle in each coordinate direction respectively, m is the mass, and f_i represents the sum of forces acting on the particle in the i direction. To determine an adequate expression for f_i, we utilize empirical and analytical formulas with an elastic collision scheme for particle-wall contact.

A. Momentum Equation for an Inertial Particle

The total force on a solid particle, f_i in Eq. (4), can be composed of three different parts: (1) Gravitational or other body forces; (2) Surface forces exerted by the fluid, such as drag or lift; and (3) Forces due to interaction with other particles and collisions with physical boundaries within the flow.

These forces represent the transfer of momentum between the two phases, which controls the complex real-life motion of fluid and solid particles. Empirical relations of drag, lift, gravity, and added mass effect for spherical non-rotating particles are considered in this model [20].

The drag force is obtained from dimensional analysis with a drag coefficient C_D, calculated as a function of the particle Reynolds number [21]:

$$C_D = \frac{24}{Re_r}\left(1 + 0.15\ Re_r^{0.687}\right) \tag{5}$$

where Re_r depends on the diameter and the relative velocity of the particle, $\mathbf{v}_r$:

$$Re_r = \frac{|\mathbf{v}_r|\, d}{\nu} \tag{6}$$

Models for lift and added mass forces in inviscid flows [22], with coefficients C_L and C_m respectively, are employed to derive the non-dimensional momentum equation, which is scaled with the container radius, and the magnitude of the rotational velocity Ω:

$$\begin{aligned}\frac{dv_{pi}}{dt} \;=\; & \frac{1}{(SG + C_m)}\left[-\frac{\delta_{i3}}{Fr^2\ \tilde{d}} + \frac{SG}{St}v_{ri}\right. \\ & \left. + C_L(\epsilon_{ijk}v_{rj}\omega_k) + (1 + C_m)\frac{Du_i}{Dt}\right]\end{aligned} \tag{7}$$

where $\tilde{d}$ is the non-dimensional particle diameter, and v_{pi} and u_i represent the i component of the particle and flow velocity. The relative velocity is defined as $v_{ri} = u_i - v_{pi}$, and the vorticity of the flow is the curl of the velocity field $\omega_i = \epsilon_{ijk}\frac{\partial u_k}{\partial x_j}$.

Other three dimensionless parameters appear in Eq.(7): The ratio of solid and fluid densities called specific gravity $SG = \rho_s/\rho$, the densimetric Froude number, which relates the inertial and gravity forces:

$$Fr = \frac{\Omega R}{\sqrt{(SG - 1)gd}} \tag{8}$$

and the Stokes number, St, used to identify the dynamical relation between the two phases. Since the drag is the dominant force, the Stokes number is defined as the ratio between the particle response time and the characteristic time scale of the flow in the container:

$$St = \frac{\tau_R}{\tau_F} = \frac{4}{3}\frac{d\ SG}{C_D\,|\mathbf{v}_r|}\Omega \tag{9}$$

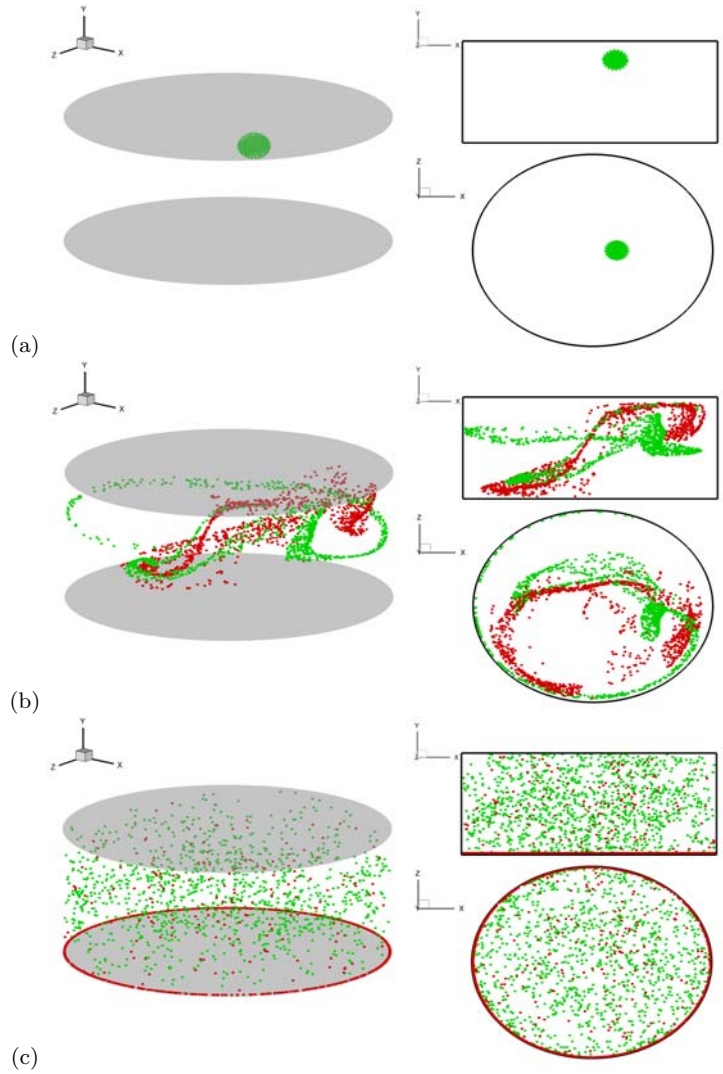

FIG. 3: Three-dimensional, side, and plan views of a group of 1250 inertial particles released in the flow. Green particles neglect the effect of gravity as $Fr \to \infty$, and red particles consider a Froude number of $Fr = 6.15$. For both simulations the additional parameters are: $Re = 350$, $AR = 1$, $\tilde{d} = 0.02$, and $SG = 2.65$. (a) Initial conditions for both groups at $t = 0$, (b) Particles after 4 lid rotations, and (c) Particle positions after 21 lid rotations.

This parameter reflects the particle behavior due to the flow caracteristics. If the value of $St \ll 1$ a particle has enough time to respond to changes in flow velocity, and it can follow closely the motion of the largest scales of the flow. On the other hand, if $St \gg 1$ the particle velocity is not affected by the flowfield, and trajectories of fluid and solid particles with the same initial conditions diverge very rapidly.

Besides particle rotation, the model given by Eq. (7) also neglects the Basset history force due to the viscous stresses on the particle surface, as well as the Faxén correction on the drag force that accounts for non-uniform flow effects [20].

B. Particle Collision Model

The boundary conditions play an important role in particle dynamics since the flow is contained by the solid walls of the cylinder. The inertial particles can make contact with the boundaries altering their momentum and trajectory, which is modeled by a collision algorithm that simulates the kinetic energy loss due to inelastic and friction effects.

Here we adopt a simple one-step collision model, for which the particle impulse changes before and after the impact by a factor given by the coefficient of restitution e, referred to the center of mass of the sphere.

Assuming no particle deformation or friction, the post-

collision velocities are obtained as:

$$v'_{p\hat{n}} = -ev_{p\hat{n}} \tag{10}$$

$$v'_{p\hat{t}} = v_{p\hat{t}} \tag{11}$$

where $v_{p\hat{n}}$ and $v_{p\hat{t}}$ are the particle velocities in the normal and tangential directions to the solid surface.

The perfecty elastic model used herein considers the restitution coefficient $e = 1$, for which the particle preserves its tangential and normal momentum.

III. ONE-WAY FLOW SIMULATIONS

The trajectory and momentum Eqs.(3) and (4), describe the particle with a point-volume representation such that all the forces are concentrated on a point that corresponds to its center of mass, and the continuum background fluid is not affected by the particle motion. These are called *one-way coupling* simulations, since the solid phase does not alter the dynamics of the fluid.

A resolved particle scheme would require a detailed modeling of the particle volume and fluid interaction, which can be simulated using boundary interface methods [26]. Recently, Hwang *et al.* [27] showed how a particle can change the surrounding flow, and generate chaotic motions in a simple two-dimensional lid-driven cavity flow.

To study the interaction of inertial particles with the flow and compare their motion with passive fluid particles, we examine the effect of inertia by separating the gravity force from the forces generated by fluid-solid contact. Poincaré maps are constructed to visualize the global Lagrangian dynamics of inertial particles, and stirring is analyzed qualitative and quantitatively from the variance of particle concentration and Lagrangian averages.

A. Effects of gravity on the particle dynamics

To analyze separately the effects of inertia and gravity, we compute the trajectories and velocities of 1250 particles without the gravity term ($Fr \to \infty$), and also with a Froude number of $Fr = 6.15$, as shown in Fig. 3.

From the simulations we observe that without gravity, the shear layer instability contributes to the stretching and folding of particle trajectories, and even though the inertial particle motion is different from the passive fluid particles trajectories, the unmixed islands visualized for the fluid motion still persist, as shown in the Poncaré sections depicted in Fig. 4.

Gravity, however, introduces a drift in the vertical direction, which depends on the magnitude of the Froude number. For a sufficiently small Fr, the inertial effects cannot maintain the particle suspension and all the flow

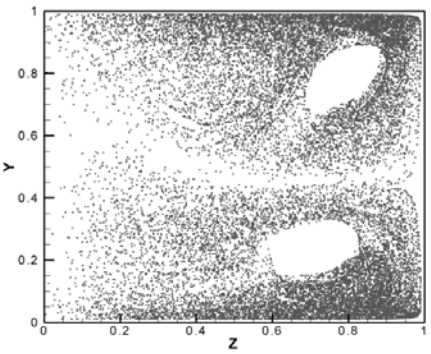

(a)

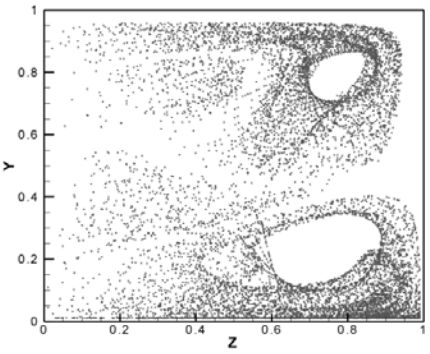

(b)

FIG. 4: Poincaré sections at $x = 0$. (a) Neglecting gravity force ($Fr \to \infty$) the unmixed islands can still be observed, and (b) Section with $Fr = 6.15$, all trajectories converge to the lower right corner of the container.

structure starts to break down, destroying the mixing process when sedimentation takes place.

The Poincaré section constructed for this case is less dense, since all the particles from different initial conditions land eventually at the bottom lid. They are pushed away to the corner by the centrifugal acceleration, and remain trapped because gravity is larger than drag or lift forces, which prevents particle escape or entrainment to the flow.

From these simulations we can deduce that for each Reynolds number, there should be a minimum Fr, such that chaotic motion of inertial particles is not suppressed. Further analysis will have to consider the inertial and body force effects separately to understand the dispersion mechanisms of a particle cloud due to transfer of low momentum only.

B. Flow topology and chaotic dynamics

To identify in detail the structures present in the complex three-dimensional flow, Lackey [11] calculated Lagrangian average maps in the transverse section of the

cylinder at a constant angle.

The Lagrangian averages are constructed by simulating the velocities and trajectories of 10,000 particles initially released in the section, and calculating the relative difference of the velocity magnitude with the average velocity of the entire flow:

$$\tilde{u}^L(i,j) = \frac{u^L(i,j) - \langle u \rangle}{\langle u \rangle} \tag{12}$$

where $u^L(i,j)$ is the Lagrangian average along the trajectory of the particle starting from the position (i,j), and $\langle u \rangle$ is the average velocity magnitude of the flowfield.

In regions where the flow is chaotic, particles cover ergodically the domain and sample all the velocities in the flow, thus Lagrangian averages of chaotic trajectories are close to zero in the passive fluid particle case.

As shown in Fig. 6 the contours of the average maps reveal the breaking of the axisymmetric flow, which produces a chaotic region where $\tilde{u}^L(i,j) \approx 0$. The Lagrangian maps also show that the size of the lower torus decreases for the inertial particle case. Quasi-periodic orbits embedded within the toroidal regions become unstable since they cannot maintain the same trajectories of fluid particles in low momentum regions. The momentum transfer decreases in some sections of the orbit, and the flow cannot overcome the particle inertia, allowing the escape due to Stokes number effects.

The same explanation can be argued for the integrable sections near the centerline, where smaller velocities are incapable of maintaining the organized motion.

The Lagrangian average maps plotted in Fig. 6 also show that for the inertial particle case, weaker invariant bands appear over the torus, in a zone that is well-mixed from the fluid particles point of view.

Since these sections were not observed in the Poincaré map of the constant azimuthal plane, we construct a new section by taking one-sixth of the cylinder, due to the symmetry of the flow, crossed by a diagonal plane as shown in Fig. 5.

In this section we observe additional unmixed zones which determine that mixing decreases for the combination of parameters employed in the simulations.

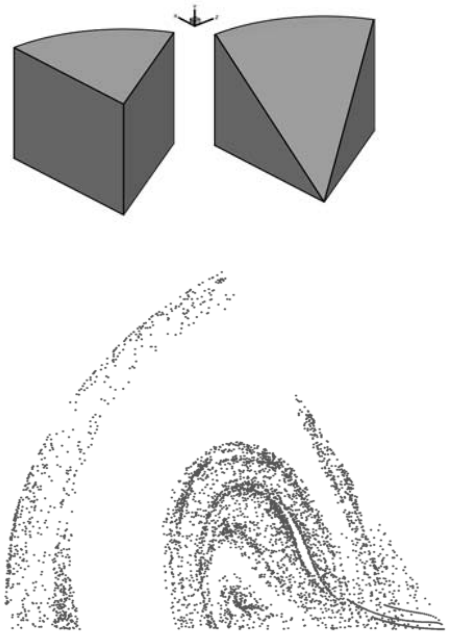

(a)

(b)

FIG. 5: Poincaré section in a transverse plane. (a) One-sixth of the geometry before and after being intersected by the plane, and (b) Poincaré section which could explain the banded zones in the Lagrangian average map.

C. Stirring inertial particles

The effects of the phenomena previously described on the Stokes number effect has a consequence on inertial particle stirring, which can be quantified with the variance of concentration [11] that corresponds to the second moment of the number of particles contained in a two-dimensional plane at an instant in time, obtained by collapsing the θ direction of the cylindrical grid.

This statistic is based on the concentration of particles at every grid point:

$$\sigma_c^2(t) = \frac{1}{I \times J} \sum_i^I \sum_j^J (C^t(i,j) - \bar{C}(t))^2 \tag{13}$$

where I and J are the maximum number of grid nodes in the r and z directions respectively, and the instantaneous mean concentration is calculated as:

$$\bar{C}(t) = \frac{1}{I \times J} \sum_i^I \sum_j^J C^t(i,j) \tag{14}$$

The variance of concentration for inertial particles with no gravity, assuming the parameters $Re = 350$, $AR = 1$, $\tilde{d} = 0.02$, and $SG = 2.65$, gives a value of $\sigma_c^2 = 3.15$ after 40 lid rotations, which is smaller than the variance of concentration of fluid particles at the same Reynolds number, which gives a value of $\sigma_{cf}^2 = 1.0$, confirming the effect of inertia on mixing.

D. Particle dispersion and periodic orbits in the tori

(*this section is still incomplete!*) To study the size variation of the cloud we can calculate the particle dispersion, which is the second-order moment of the particle position in each coordinate direction that reflects the displacement of particles due to inertial effects.

Wang *et al.* [15] calculated a dispersion coefficient from numerical experiments, based on Taylor's stochastic theory of turbulent diffusion. In this analysis the dispersion

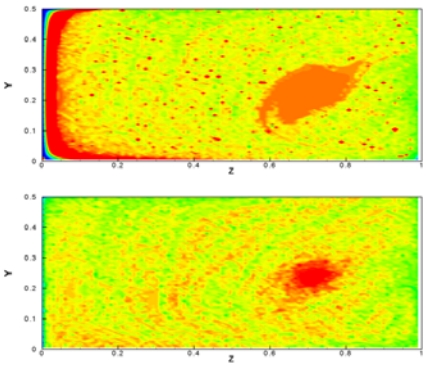

FIG. 6: Lagrangian average maps at $x = 0$. (a) Average map of fluid particles showing the section of the torus and integrable section at centerline, and (b) Map for inertial particles. Integrable sections decrease, but banded zones appear on the mixing section.

depends on the autocorrelation function of the velocity field as:

$$\frac{1}{2}\frac{d}{dt}\langle x_{pij}^2\rangle = \int_0^\infty \langle u_{pi}(t)u_{pj}(t+\tau)\rangle d\tau \qquad (15)$$

Fig. 7 shows the autocorrelation function of the velocity on the x-direction for one of the particles shown in Fig. 3. The time dependence structure is periodic due to the forcing imposed by the lids, which can be removed to observe the real loss of information of the particle in time in all three coordinate directions. The area under these curves would represent the growth rate of $\langle x_{pij}^2\rangle$ in time.

This information can also be obtained from periodic orbit theory [17]. Using the flow characteristics observed in the Poincaré section and Lagrangian average map, we approximate the fixed points and orbits, depicted in Fig. 8, tracking particles with initial conditions at the center of both tori, and at the center and corners where the minimum values of the Lagrangian averages are located.

The relevant transverse eigenvalues on the periodic orbits are obtained by integrating the Jacobian as shown in appendix A. The corresponding maximum values are $\Lambda_p = 0.170$ in both orbits, which indicates their local unstable character.

With the purpose of calculating the particle dispersion in time, or the square of the particle distance with respect to the mean, we can also use the information provided by the spectrum of periodic orbits in the flow.

Using the contribution of a few prime cycles we can calculate the trace of the evolution operator, or the zeros of the following spectral determinant [17]:

$$\det(s-A) = \exp\left[-\sum_p \sum_r \frac{1}{r}\frac{e^{r(\beta A_p - sT_p)}}{\left|\det\left(\mathbf{I}-\mathbf{J}_p^r\right)\right|}\right] \qquad (16)$$

which can also be obtained through the leading zeros of

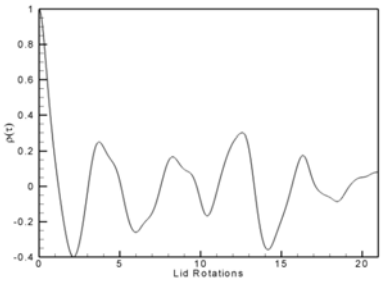

FIG. 7: Autocorrelation function of the u velocity of an inertial particle. The dependence shows the periodicity due to the rotation of the lids.

the dynamical zeta function:

$$\frac{1}{\zeta} = \prod_p (1-t_p) \qquad (17)$$

where $t_p = e^{\beta A_p - sT_p}/\left|\Lambda_p\right|$. The integral of the observable (particle position in this case) is contained in A_p, T_p is the period of the orbit, and β the auxiliary variable of the generating function.

IV. CONCLUDING REMARKS

The numerical investigation of Lackey [11], demonstrated that the steady flow in a cylindrical container with exactly counter-rotating lids, for $AR = 1$, becomes three-dimensional due to the shear layer instability developed at the central plane, at a sufficiently large Reynolds number.

In this investigation we study the dynamics of inertial particles in this flow, to understand how chaotic regions contribute to particle stirring when the specific gravity and size of the dispersed phase are important.

The momentum equation (7), based on analytical and empirical relations of surface and body forces, is solved with an elastic collision scheme to account for particle-wall interactions.

One-way coupling simulations showed that at a given Re, the gravity force can suppress particle stirring when the Froude number decreases. Further analyses without gravity showed that integrable regions observed in fluid motion still persist, but decrease due to inertial effects.

Even though the diameter of the unmixed islands observed in Poincaré sections and Lagrangian average maps becomes smaller, the variance of particle concentration evidenced a reduced mixing in the inertial particle case. This phenomenon occurs since in certain regions of the flow the intrinsic time-scale of the particles is larger than the time-scale of the fluid motion, which is reflected on the magnitude of the Stokes number.

Several new aspects of the dynamics of inertial particles in rotating flows have been found, and require further

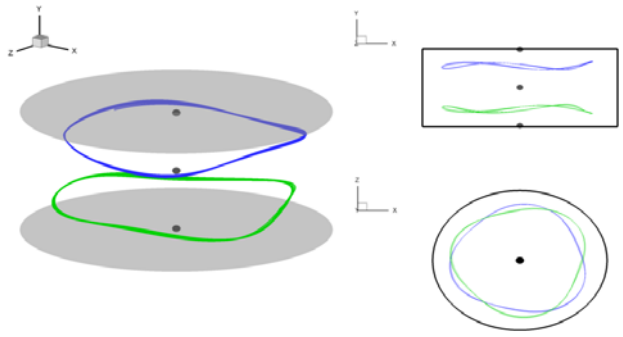

FIG. 8: Fixed points and orbits within the invariant region of inertial particles.

investigation to evaluate in detail the dependence on the parameters defined in the equations.

Chaotic advection and periodic orbit theory can help to explore the complex flow and find results of physical relevance, to design experiments and clarify the dynamics of the two-phase interaction in these flows.

Acknowledgments

I would like to thank Tahirih Lackey for providing me the documentation of her thesis, and Predrag Cvitanović and Fotis Sotiropoulos for numerous helpful suggestions.

APPENDIX A: JACOBIAN AND EIGENVALUES CALCULATION

Defining the state space vector of an inertial particle as:

$$\mathbf{x} = [u_p \; v_p \; w_p \; x_p \; y_p \; w_p]^T \tag{A1}$$

the right hand side of the system is expressed in the following vector:

$$\boldsymbol{v} = [f_1/m \; f_2/m \; f_3/m \; u_p \; v_p \; w_p]^T \tag{A2}$$

Therefore, the matrix of variations of the flow is:

$$\mathbf{A} = \begin{bmatrix} \frac{\partial v_1}{\partial x} & \frac{\partial v_1}{\partial y} & \frac{\partial v_1}{\partial z} & 0 & 0 & 0 \\ \frac{\partial v_2}{\partial x} & \frac{\partial v_2}{\partial y} & \frac{\partial v_2}{\partial z} & 0 & 0 & 0 \\ \frac{\partial v_3}{\partial x} & \frac{\partial v_3}{\partial y} & \frac{\partial v_3}{\partial z} & 0 & 0 & 0 \\ 1 & 0 & 0 & 0 & 0 & 0 \\ 0 & 1 & 0 & 0 & 0 & 0 \\ 0 & 0 & 1 & 0 & 0 & 0 \end{bmatrix} \tag{A3}$$

We obtain the eigenvalues of the Jacobian, on the periodic orbits, by integrating the system:

$$\frac{d\mathbf{J}}{dt} = \mathbf{A}\mathbf{J} \tag{A4}$$

where the components are obtained from the derivatives of the particle forces, Eq.(7):

$$\begin{aligned}
\frac{\partial v_1}{\partial x} &= -\frac{SG}{St}\left\{1 - \frac{u_r \Omega R}{C_D}\right. \\
&\left.\left[\frac{C_D u_r}{|\mathbf{v}_r|^2} - \frac{Re_p u_r}{|\mathbf{v}_r|}\left(\frac{24}{Re_r} + \frac{1.1268}{Re_r^{1.313}}\right)\right]\right\} \\
&\frac{1}{(SG + C_m)} \\
\frac{\partial v_1}{\partial y} &= \left\{\frac{SG}{St}\frac{u_r \Omega R}{C_D}\left[\frac{C_D v_r}{|\mathbf{v}_r|^2}\right.\right. \\
&\left.\left. - \frac{Re_p v_r}{|\mathbf{v}_r|}\left(\frac{24}{Re_r} + \frac{1.1268}{Re_r^{1.313}}\right)\right] - C_L \omega_z\right\}\frac{1}{(SG + C_m)} \\
\frac{\partial v_1}{\partial z} &= \left\{\frac{SG}{St}\frac{u_r \Omega R}{C_D}\left[\frac{C_D w_r}{|\mathbf{v}_r|^2}\right.\right. \\
&\left.\left. - \frac{Re_p w_r}{|\mathbf{v}_r|}\left(\frac{24}{Re_r} + \frac{1.1268}{Re_r^{1.313}}\right)\right] + C_L \omega_y\right\}\frac{1}{(SG + C_m)} \\
\frac{\partial v_2}{\partial x} &= \left\{\frac{SG}{St}\frac{v_r \Omega R}{C_D}\left[\frac{C_D u_r}{|\mathbf{v}_r|^2}\right.\right. \\
&\left.\left. - \frac{Re_p u_r}{|\mathbf{v}_r|}\left(\frac{24}{Re_r} + \frac{1.1268}{Re_r^{1.313}}\right)\right] + C_L \omega_z\right\}\frac{1}{(SG + C_m)} \\
\frac{\partial v_2}{\partial y} &= -\frac{SG}{St}\left\{1 - \frac{v_r \Omega R}{C_D}\right. \\
&\left.\left[\frac{C_D v_r}{|\mathbf{v}_r|^2} - \frac{Re_p v_r}{|\mathbf{v}_r|}\left(\frac{24}{Re_r} + \frac{1.1268}{Re_r^{1.313}}\right)\right]\right\} \\
&\frac{1}{(SG + C_m)} \\
\frac{\partial v_2}{\partial z} &= \left\{\frac{SG}{St}\frac{v_r \Omega R}{C_D}\left[\frac{C_D w_r}{|\mathbf{v}_r|^2}\right.\right. \\
&\left.\left. - \frac{Re_p w_r}{|\mathbf{v}_r|}\left(\frac{24}{Re_r} + \frac{1.1268}{Re_r^{1.313}}\right)\right] - C_L \omega_x\right\}\frac{1}{(SG + C_m)} \\
\frac{\partial v_3}{\partial x} &= \left\{\frac{SG}{St}\frac{w_r \Omega R}{C_D}\left[\frac{C_D u_r}{|\mathbf{v}_r|^2}\right.\right. \\
&\left.\left. - \frac{Re_p u_r}{|\mathbf{v}_r|}\left(\frac{24}{Re_r} + \frac{1.1268}{Re_r^{1.313}}\right)\right] - C_L \omega_y\right\}\frac{1}{(SG + C_m)} \\
\frac{\partial v_3}{\partial y} &= \left\{\frac{SG}{St}\frac{w_r \Omega R}{C_D}\left[\frac{C_D v_r}{|\mathbf{v}_r|^2}\right.\right. \\
&\left.\left. - \frac{Re_p v_r}{|\mathbf{v}_r|}\left(\frac{24}{Re_r} + \frac{1.1268}{Re_r^{1.313}}\right)\right] + C_L \omega_x\right\}\frac{1}{(SG + C_m)} \\
\frac{\partial v_3}{\partial z} &= -\frac{SG}{St}\left\{1 - \frac{w_r \Omega R}{C_D}\right. \\
&\left.\left[\frac{C_D w_r}{|\mathbf{v}_r|^2} - \frac{Re_p w_r}{|\mathbf{v}_r|}\left(\frac{24}{Re_r} + \frac{1.1268}{Re_r^{1.313}}\right)\right]\right\} \\
&\frac{1}{(SG + C_m)}
\end{aligned}$$

where $Re_p = \Omega R d/\nu$.

From matrix **A**, we identify two zero eigenvalues, three unit eigenvalues when we integrate along a periodic orbit, and a transverse eigenvalue Λ_p.

[1] J. M. Ottino, "Mixing, chaotic advection, and turbulence", *Annual Rev. Fluid Mech.* **22**, 207-253 (1990).

[2] H. Aref, "Stirring by chaotic advection", *J. of Fluid Mechanics* **143**, 1-21 (1984).

[3] T. Dombre *et al.*, "Chaotic streamlines in ABC flows", *J. of Fluid Mechanics* **167**, 353-391 (1986).

[4] W. L. Chien, H. Rising, and J. M. Ottino, "Laminar mixing and chaotic mixing in several cavity flows", *J. of Fluid Mechanics* **170**, 355-377 (1986).

[5] D. Beige, A. Leonard, and S. Wiggins, "Laminar mixing and chaotic mixing in several cavity flows", *Chaos, Solitons, and Fractals* **4**, 749-868 (1994).

[6] D. Rothstein, E. Henry, and J. P. Gollub, "Persistent patterns in transient chaotic fluid mixing", *Nature* **401**, 770-772 (1999).

[7] H. Aref, "The development of chaotic advection", *Phys. of Fluids* **14**, 1315-1325 (2002).

[8] T. H. Solomon and I. Mezić, "Uniform resonant chaotic mixing in fluid flows", *Nature* **425**, 376-380 (2003).

[9] F. Sotiropoulos, Y. Ventikos, and T. C. Lackey, "Chaotic advection in three-dimensional stationary vortex-breakdown bubbles: Šil'nikov's chaos and the devil's staircase", *J. of Fluid Mechanics* **444**, 257-297 (2001).

[10] F. Sotiropoulos, D. R. Webster, and T. C. Lackey, "Experiments on Lagrangian transport in steady vortex-breakdown bubbles in a confined swirling flow", *J. of Fluid Mechanics* **466**, 215-248 (2002).

[11] T. C. Lackey, *Numerical investigation of chaotic advection in three-dimensional experimentally realizable rotating flows*, PhD Thesis, Georgia Institute of Technology, (2004).

[12] C. Nore *et al.*, "The 1:2 mode interaction in exactly counter-rotating von Kárman swirling flow", *J. of Fluid Mechanics* **477**, 51-88 (2003).

[13] C. Nore *et al.*, "Survey of instability thresholds of flow between exactly counter-rotating disks", *J. of Fluid Mechanics* **511**, 45-65 (2004).

[14] I. Mezić, "Chaotic advection in bounded Navier-Stokes flows", *J. of Fluid Mechanics* **431**, 347-370 (2001).

[15] L. P. Wang *et al.*, "Chaotic dynamics of particle dispersion in fluids", *Phys. Fluids A* **4**, 1789-1804 (1992).

[16] Y. Tsega, E. E. Michaelides, and E. V. Eschenazi, "Laminar mixing and chaotic mixing in several cavity flows", *Chaos* **11**, 351-358 (2001).

[17] P. Cvitanović *et al.*, *Chaos: Classical and Quantum*, advanced graduate e-textbook, `ChaosBook.org` (Niels Bohr Institute, Copenhagen 2005).

[18] J. M. Lopez *et al.*, "Instability and mode interactions in a differentially driven rotating cylinder", *J. of Fluid Mechanics* **462**, 383-409 (2002).

[19] F. Moisy, T. Pasutto, and M. Rabaud, "Instability patterns between counter-rotaing disks", *Nonlin. Proc. in Geophysics* **10**, 281-288 (2003).

[20] C. T. Crowe, T. R. Troutt, and J. N. Chung, *Multiphase Flows with Droplets and Particles*, (CRC Press, 1998).

[21] L. Shiller, and A. Naumann, "Über die Grundlegenden Berechungen bei der Schwerkraftaufbereitung", *Ver. Deutsh. Ing.* **77**, 318 (1933).

[22] T. R. Auton, J. C. R. Hunt, and M Prud'homme, "The force exerted on a body in inviscid unsteady non-uniform rotational flow", *J. of Fluid Mechanics* **197**, 241-257 (1988).

[23] L. P. Wang, T. D. Burton, and D. E. Stock, "Chaotic dynamics of heavy particle dispersion: Fractal dimension versus dispersion coefficients", *Phys. Fluids A* **2**, 1305-1308 (1990).

[24] M. R. Maxey, "On the advection of spherical and non-spherical particles in a non-uniform flow", *Phil. Trans: Phys. Sci. and Eng.* **333**, 289-307 (1990).

[25] L. P. Wang, T. D. Burton, and D. E. Stock, "Quantification of chaotic dynamics for heavy particle dispersion in ABC flow", *Phys. Fluids A* **3**, 1073-1080 (1991).

[26] A. Gilmanov, F. Sotiropoulos, and E. Balaras, "A general reconstruction algorithm for simulating flows with complex 3D immersed boundaries on Cartesian grids", *J. Comput. Phys.* **191**, 660-669 (2003).

[27] W. R. Hwang, P. D. Anderson, and M. A. Hulsen, "Chaotic advection in a cavity flow with rigid particles", *Phys. of Fluids* **17**, 043602 (2005).